communications physics

Article

https://doi.org/10.1038/s42005-024-01779-3

Constraints on fifth forces and ultralight dark matter from OSIRIS-REx target asteroid Bennu

Check for updates

Yu-Dai Tsai [1,2,3,4] ✉, Davide Farnocchia [5], Marco Micheli [6], Sunny Vagnozzi [7,8] & Luca Visinelli [9,10] ✉

It is important to test the possible existence of fifth forces, as ultralight bosons that would mediate these are predicted to exist in several well-motivated extensions of the Standard Model. Recent work indicated asteroids as promising probes, but applications to real data are lacking so far. Here we use the OSIRIS-REx mission and ground-based tracking data for the asteroid Bennu to derive constraints on fifth forces. Our limits are strongest for mediator masses $m \sim (10^{-18}\text{-}10^{-17})$ eV, where we currently achieve the tightest bounds. These can be translated to a wide class of models leading to Yukawa-type fifth forces, and we demonstrate how they apply to $U(1)_B$ dark photons and baryon-coupled scalars. Our results demonstrate the potential of asteroid tracking in probing well-motivated extensions of the Standard Model and ultralight bosons near the fuzzy dark matter range.

Anomalies in the trajectories of objects across the sky have often led to the discovery of new physical laws or celestial bodies. The planet Neptune was inferred based on the irregularities of the orbit of Uranus according to Newton's theory, and General Relativity was first confirmed with its prediction of Mercury's anomalous precession. Besides planets, other bodies in the Solar Systems that are being tracked with increasing precision include near-Earth asteroids. Currently, asteroids are tracked with plane-of-sky astrometric measures paired with line-of-sight studies by radar astrometry. Stellar occultations and the Gaia satellite also provide highly accurate astrometry.

Asteroid tracking and planetary defense are crucial missions of the National Aeronautics and Space Administration (NASA) and the European Space Agency (ESA). Consequently, a wealth of data related to the orbits of these objects is available and can be used to probe fundamental physics, including new physics beyond the Standard Model of particle physics (SM). This is the path we take in the present work, focusing on data from the Origins, Spectral Interpretation, Resource Identification, Security, Regolith Explorer (OSIRIS-REx) mission. OSIRIS-REx is a NASA space mission designed to study the potentially hazardous asteroid (101955) Bennu. The spacecraft is equipped with several scientific instruments, including a camera suite, a laser altimeter, and a spectrometer, which allowed it to map Bennu's surface and study its composition, geology, and mineralogy, as well as improve the knowledge Bennu's future trajectory to reassess the probability of a future impact on Earth[1]. Launched in 2016, the OSIRIS-REx spacecraft arrived at the near-Earth asteroid Bennu and began conducting scientific observations and measurements in December 2018, before performing a Touch-and-Go (TAG) sample acquisition maneuver in October 2020, during which a sample of carbonaceous regolith of at least 60 g was collected and returned to Earth for analysis in September 2023[2].

Overall, the OSIRIS-REx mission has provided an exciting opportunity for scientists to explore and study one of the most primitive objects in the solar system, and to gain insights into the history and evolution of our cosmic neighborhood. The OSIRIS-REx tracking data are archived in the Small Bodies Node of the Planetary Data System, see ref. 3. The data has been used to track to exquisite precision the trajectory of the asteroid Bennu, measure the Yarkovsky effect acting on it, and refine the long-term impact hazard for the asteroid[4].

Asteroid tracking can be invoked to test theories of gravity such as the validity of Newton's inverse square law. In fact, the laws of gravity would be modified if a new (ultra)light field exists in Nature, due to the capability for such a field to act as a "fifth force" and modify the orbits of larger bodies. The possibility of the existence of hidden fifth forces, in addition to those included in the SM, as well as the weakly coupled ultralight particles that mediate these forces, are topics of extreme importance in modern particle

[1]Los Alamos National Laboratory (LANL), Los Almos, NM, USA. [2]Department of Physics and Astronomy, University of California, Irvine, CA, USA. [3]Fermi National Accelerator Laboratory (Fermilab), Batavia, IL, USA. [4]Kavli Institute for Cosmological Physics (KICP), University of Chicago, Chicago, IL, USA. [5]Jet Propulsion Laboratory (JPL), California Institute of Technology, Pasadena, CA, USA. [6]European Space Agency (ESA) NEO Coordination Centre, Frascati (RM), Italy. [7]Department of Physics, University of Trento, Povo (TN), Italy. [8]Trento Institute for Fundamental Physics and Applications (TIFPA)-INFN, Povo (TN), Italy. [9]Tsung-Dao Lee Institute (TDLI), Shanghai, China. [10]School of Physics and Astronomy, Shanghai Jiao Tong University, Shanghai, China. ✉e-mail: yt444@cornell.edu; ytsai@fnal.gov; luca.visinelli@sjtu.edu.cn

physics. Among others, these light particles are natural candidates for the dark matter and dark energy, and appear ubiquitously within string theory[5–7]. Fifth forces mediated by a new light bosonic field appear in extensions of the SM and, more generally, in beyond the SM (BSM) models that attempt to incorporate the observed dark matter and dark energy contents into a general framework. Many motivated BSM models in this sense have been studied in the literature, and include the gauged $U(1)_B$[8], $U(1)_{B\text{-}L}$[9], $L_\mu - L_{e,\tau}$[10], baryon-coupled scalar[11,12], and massive gravity[13–15] models.

A wide range of probes have been used to search for and constrain hidden fifth forces and ultralight particles, including but not limited to laboratory and space tests, cosmological and astrophysical observations[16–20]. Among others, the Lunar Laser Ranging (LLR) is monitoring the distance between the Moon and Earth with millimetric precision, placing strong bounds on the time variability of Newton's constant and on the strong equivalence principle[21]. Proof-of-principle studies have been discussed as possible ways to place model-dependent limits on a novel fifth force using asteroid and planetary precessions[22,23]. The data has also been used to obtain constraints on the local dark matter and cosmic neutrino densities[24]. Planetary ephemerides released by the Observatory of Paris and the Côte d'Azur Observatory (INPOP)[25,26] have also been used to constrain fifth-force ranges[27] and the effects of a non-zero mass for the graviton[28].

In this paper, we conduct a robust search for a hypothetical fifth force with precision asteroid tracking. To reach our goal, we utilize data for the orbit of Bennu from the OSIRIS-REx mission[4]. We also considered a second asteroid, namely (99942) Apophis, which was extensively tracked with ground-based optical and radar telescopes from 2004 to 2021. Apophis will be visited by the extended OSIRIS-REx mission, OSIRIS-APEX[29], which may further improve the constraints reported here. We select a few simple and well-motivated realizations of the existing BSM models to demonstrate the power of our constraints. Nevertheless, it is straightforward to map the parametrization adopted here to other models that lead to a Yukawa-type fifth force among those mentioned above, see, e.g., ref. 30.

In summary, here we constrain the couplings of fifth forces and ultralight bosons in Yukawa-type fifth forces. The bounds derived use the OSIRIS-REx mission and ground-based tracking data for the asteroid Bennu, and are strongest for mediator masses $m \sim (10^{-18}\text{–}10^{-17})$ eV. We demonstrate how the bounds translate to $U(1)_B$ dark photons and baryon-coupled scalars. Our results demonstrate the potential of asteroid tracking in probing well-motivated extensions of the Standard Model and ultralight bosons close to the fuzzy dark matter range. Unless otherwise specified, throughout the paper, we use natural units ($\hbar = c = 1$), where $\hbar$ is the reduced Planck's constant and c is the speed of light.

Methods

Fifth forces and motion of celestial objects

A number of scenarios beyond the SM, including but not limited to those mentioned in the Introduction, predict the existence of new (ultra)light particles, which would mediate a new, long-ranged, fifth force. For example, the SM contains a number of Abelian or $U(1)$ global symmetries, which are treated as "accidental" symmetries, which should be spoiled by the appearance of UV-completing operators such as those arising in quantum gravity[31,32]. For this, a $U(1)$ symmetry can be promoted to a gauge symmetry that is spontaneously broken below some UV energy scale, with the corresponding gauge boson ϕ in the case of a scalar field, or a vector field A' in the case of an axial vector gauge. Examples include models based on new (gauged) symmetries such as gauged baryon number conservation $U(1)_B$, $U(1)_{B\text{-}L}$, $L_\mu - L_{e,\tau}$ as well as baryon-coupled scalars. For the case of $L_\mu - L_e$, the presence of plasma would lead to an effective screening of the fifth force mediated by the gauge boson. In this case, the effective coupling to electrons $g_{e,\text{eff}}$ would be lower than the actual (Lagrangian) gauge coupling g_e. Accounting for this effect would require a careful modeling of the plasma number density in the Solar System, and is therefore quite challenging. In our case, since we are focusing on $U(1)_B$, plasma effects are unimportant. In addition, a kinetic mixing interaction between the SM photon and a new vector boson is, in general, allowed[33]. However, this would lead to non-gravitational interactions, which are expected to be unimportant for what concerns the orbits of celestial objects, especially when considering the very tight upper limits on the kinetic mixing strength ϵ. For these reasons, in what follows we neglect the effect of a possible kinetic mixing interaction.

A light scalar field ϕ of mass m_ϕ introduces a new channel through which particles can exchange momentum $\mathbf{q}$ and scatter with an amplitude $|\mathcal{M}| \propto 1/(q^2 + m_\phi^2)$, where $q = |\mathbf{q}|$. The fifth force potential associated with this scattering amplitude is of the Yukawa type[34], with the boson mass providing a cutoff over which the force extends, whereas the details concerning the force coupling depend on the charge and spin structure of the particles involved in the scattering process. Likewise, some models predict the fifth force to be mediated by a hidden vector particle A' of mass $m_{A'}$, often referred to as a dark photon. A review of tests on the modification of gravity that includes Yukawa-type forces can be found in ref. 35. When describing the methods, we will refer to a scalar field ϕ of mass m_ϕ, although the results can also be extended to contemplate the vector case.

The presence of a long-range Yukawa-type force leads to deviations from Newton's inverse square law, which can be tested and constrained. In fact, given a specific theory that contains a gauge symmetry, any body would acquire a charge Q associated with the breaking of the gauge symmetry, so that the mutual interaction between two bodies of charges Q_1 and Q_2 at a distance r reads:

$$V(r) = \mp(\hbar c)\frac{g^2}{4\pi}\frac{Q_1\,Q_2}{r}\exp\left(-\frac{m_\phi c}{\hbar}r\right), \tag{1}$$

where g is the coupling strength associated with the gauge field. Given the position $\mathbf{r}$ of the celestial object with respect to the Sun, the central potential only depends on the radial coordinate $r = |\mathbf{r}|$. This is a very generic parametrization that encompasses a number of interesting scenarios. This result has profound implications for the motion of celestial objects around the Sun.

The effect of the fifth force in Eq. (1) due to a mediator of mass m_ϕ through the central potential in the model proposed translates as:

$$V(r) = \widetilde{\alpha}\,\frac{GM_\odot M_*}{r}\exp\left(-\frac{r}{\lambda}\right), \tag{2}$$

where $\widetilde{\alpha}$ characterizes the strength of the fifth force, and $\lambda = \hbar/(m_\phi c)$ is the fifth force range. In what follows, we specialize the discussion to an asteroid of mass M_* orbiting in the solar system under the influence of the Sun of mass $M_\odot$. The conversion between the coupling g associated to the gauge group and appearing in Eq. (1), and $\widetilde{\alpha}$ appearing in Eq. (2), depends on the specific microphysical model underlying the fifth force (see e.g., refs. 36,37). For instance, in the case of a gauged $U(1)_B$ model, the charges under the specific gauge group of the Sun and the celestial body result in $Q_\odot = M_\odot/m_p$ and $Q_* = M_*/m_p$, respectively, with m_p denoting the proton mass. Combining Eqs. (1), (2), and temporarily restoring SI units, we find that the conversion between $\widetilde{\alpha}$ and the coupling in the gauge model g_B is:

$$\widetilde{\alpha} = \frac{\hbar c}{G}\frac{g_B^2}{4\pi m_p^2}\,. \tag{3}$$

From entirely analogous considerations, in the case of a gauged $U(1)_{B\text{-}L}$ model, the conversion between $\widetilde{\alpha}$ and $g_{B\text{-}L}$ is as follows:

$$\widetilde{\alpha} = \frac{\hbar c}{G}\left(\frac{A-Z}{A}\right)_\odot\left(\frac{A-Z}{A}\right)_*\frac{g_{B-L}^2}{4\pi m_p^2}\,, \tag{4}$$

where Z and A are the mass-weighted atomic number and mass number respectively. The expression above implies:

$$g_B = g_{B-L}\sqrt{\left(\frac{A-Z}{A}\right)_\odot\left(\frac{A-Z}{A}\right)_*}\,, \tag{5}$$

which clearly depends to some extent on the chemical and mass composition of the two objects. The mass-weighted value of the term $(A - Z)/A$ is typically of the order of ~ 0.5, although for specifically designed materials, this ratio can be significantly different from 1, see ref. 37.

In this work, we shall remain as agnostic as possible for what concerns the microscopical origin of the fifth force, and will simply parameterize it in terms of $\widetilde{\alpha}$ and λ as appearing in Eq. (2). However, we emphasize that it is always possible to translate these constraints to the corresponding limits in terms of the mass and coupling of an ultralight particle, once a specific underlying fifth force model is chosen. Note that in the limit $m_\phi \to 0$, and therefore $\lambda \to +\infty$, the effects of the potential in Eq. (2) translate into a modification of Newton's constant, $G \to G(1 + \widetilde{\alpha})$. The symmetries of the problem (and in particular, the potential being central) indicate that the motion is typically planar to a very good approximation, so the coordinate system is fixed such that the polar angle is $\theta = \pi/2$.

It is useful to consider the reciprocal coordinate $u = 1/r$, in terms of which the equation of motion for the celestial object, including General Relativity (GR) corrections and temporarily restoring SI units, is given by[22,23]:

$$\frac{\mathrm{d}^2 u}{\mathrm{d}\varphi^2} + u = \frac{GM_\odot}{L^2} + \frac{3GM_\odot}{c^2}u^2 + \widetilde{\alpha}\frac{GM_\odot}{L^2}\left(1 + \frac{1}{\lambda u}\right)e^{-\frac{1}{\lambda u}}, \qquad (6)$$

where φ is the azimuthal angle that parameterizes the motion of the celestial object, L denotes the orbital angular momentum per unit mass, whereas the first, second, and third set of terms on the right-hand side describe the effects of Newtonian physics, GR corrections, and the fifth force, respectively.

In Newtonian physics, the motion of a bound object in an isolated two-body system traces out a fixed elliptical orbit; in particular, the semimajor axis of the ellipse is fixed in space. However, the last two sets of terms on the right-hand side of Eq. (6) lead to a precession (rotation) of the celestial object's perihelion as it revolves around the Sun. In other words, u changes as the azimuthal angle is shifted by $\varphi \to \varphi + 2\pi n$, or equivalently, the celestial object will return to its perihelion after one precession at an azimuthal angle which differs from 2π by a quantity $\Delta\varphi$. This precession leads to potentially observable effects in the motion of celestial objects, including but not limited to asteroids and planets.

The Newtonian solution to Eq. (6) for an asteroid in a closed orbit of eccentricity e is $u_0(\varphi) = M_\odot(1 + \mathsf{e}\cos\varphi)/L^2$. To determine the perihelion precession (measured from a fixed reference direction) per orbital period as a function of the fifth force strength and range, we can numerically solve Eq. (6) for $u(\varphi)$, expanding perturbatively around the Newtonian solution $u_0(\varphi)$, and deriving the shift in the φ-period relative to 2π, $\Delta\varphi$, from this solution (see ref. 23 and Appendix B of ref. 24 for more details).

While a closed-form expression for the contribution to the perihelion precession from fifth forces described by the potential in Eq. (2) is generally not available, an approximate expression can be obtained in the limit of a very light mediator $m_\phi \ll \hbar/ac$, i.e., when the semimajor axis a is much smaller than the fifth force range. In this case, one finds (see, e.g., ref. 23):

$$|\Delta\varphi| \simeq \frac{2\pi\widetilde{\alpha}}{1+\widetilde{\alpha}}\left(\frac{am_\phi c}{\hbar}\right)^2(1-\mathsf{e}) = \frac{2\pi\widetilde{\alpha}}{1+\widetilde{\alpha}}\left(\frac{a}{\lambda}\right)^2(1-\mathsf{e}), \qquad (7)$$

which correctly vanishes in the limit $m_\phi \to 0$, reflecting the fact that this limit simply recovers the inverse square law (or equivalently a $\propto 1/r$ potential, albeit with a different value of the gravitational constant), which does not lead to precession. Note that the perihelion precession $|\Delta\varphi|$ increases with the square of the semimajor axis under this limit, which indicates the benefit of studying objects at a relatively large distance from the Sun, such as Trans-Neptunian objects (TNOs). Such a dataset could also improve the determination of the dark matter density within the solar system performed in ref. 24, for which the perihelion precession benefits from an additional power of a compared to our case.

We utilize the state-of-the-art asteroidal orbital determination, for which meter-level tracking data can be available, to provide constraints on fifth forces. To do so, we employ the Comet and Asteroid Orbit Determination Package developed and maintained by NASA Jet Propulsion Lab (JPL), whose force models account for N-body Newtonian and relativistic gravity, oblateness terms, and nongravitational perturbations[4], supplemented with the fifth force we intend to constrain. These aspects will be discussed in more detail below.

Data and analysis

The trajectory of the asteroid Bennu has been extremely well constrained by a combination of ground-based optical and radar astrometric data collected ever since its discovery in 1999. The level to which Bennu's ephemeris is constrained was significantly improved by X-band radiometric and optical navigation tracking data collected during asteroid proximity operations by the OSIRIS-REx mission, from its arrival in December 2018 to sample collection in October 2020.

In this work, we make use of the same dataset used in the earlier Bennu ephemeris and hazard assessment analysis of ref. 4. In particular, this includes the following data, for a total of more than 17 orbital periods included in the fit (the orbit is not closed due to orbital precession, but acquires the typical "rose petal" shape—an excellent animation of Bennu's orbit from 9 August 2016 – 23 September 2023 can be found on ref. 38, refer to the green curve):

- ground-based optical astrometry data, including 489 right ascension and declination observations from 1999-09-11 to 2018-05-15, see ref. 39;
- all available ground-based radar astrometry data, collected during three close encounters in September 1999, September 2005, and September 2011 by the Arecibo and Goldstone radar stations, and comprising 7 Doppler and 22 delay measurements, see ref. 40;
- 36 geocentric pseudo-range points for Bennu's barycenter between 2019-01-03 16:56:56 UTC and 2020-10-03 19:14:18 UTC, derived from the OSIRIS-REx high-gain antenna tracking data in ref. 4 (see Table 1 from ref. 4), and for which a 15 ns uncertainty is assumed and corresponds to an uncertainty of 2 m for the radial distance between Bennu and Earth. These points have been obtained using tracking data obtained during the mission orbital phases Orbital A, B, C, and R, Reconnaissance B and C, Rehearsal, and pre-TAG (during which the OSIRIS-REx spacecraft was in a closed orbit around Bennu), and selecting independent, maneuver-free arcs of approximately 10 days, see ref. 4 for more details. See the "Data Availability" section for details on the availability of OSIRIS-REx data, shape models of Bennu, and kernels and small-force files.

All the above data was used to compute an orbit solution, as in ref. 4.

The pseudo-range points discussed above lead to a significant improvement in the determination of Bennu's trajectory. This, in turn, imposes stringent requirements on the fidelity of the underlying force model used to fit the trajectory. We adopt the same high-fidelity model developed for the purposes of the earlier Bennu ephemeris and hazard assessment analysis of ref. 4. This model accounts for (relativistic) gravitational effects from the Sun, the eight planets, Pluto, and the Moon (modeled through a first-order parametrized post-Newtonian N-body formulation, also known as Einstein-Infeld-Hoffman formulation, see refs. 41,42), point-mass Newtonian gravitational effects from 343 small-body perturbers, and gravitational effects from the Earth's oblateness, as well as a number of non-gravitational perturbation effects which include the Yarkovsky effect, solar radiation pressure, and Poynting-Robertson drag. The orbit solution is determined using the JPL Comet and Asteroid Orbit Determination Package, and employing the DIVA variable order Adams integrator to quadruple precision, with integration tolerance of 10^{-18}. For further details on the underlying force model and integration precision requirements, we refer the reader to ref. 4.

To derive fifth force constraints, the force model of ref. 4 is further expanded to include the acceleration associated with the fifth force, obtained

by differentiating Eq. (2) and dividing by the asteroid mass M_*:

$$\mathbf{a}(\mathbf{r}) = \widetilde{\alpha}\frac{GM_\odot}{r^3}e^{-\frac{r}{\lambda}}\left(1+\frac{r}{\lambda}\right)\mathbf{r}\,. \tag{8}$$

Note that in our force model, we apply the above acceleration term only to Bennu, not the other bodies: a posteriori, given the very stringent upper limits on the fifth force strength, we expect this to be a valid approximation for the range of parameter space explored.

As in ref. 4, the model parameters varied in the fit to determine the orbit solution are Bennu's heliocentric orbital elements (eccentricity, perihelion distance, time of perihelion TDB, longitude of node, argument of perihelion, and inclination) at osculating epoch 2011 January 1.0 barycentric dynamical time (TDB), Bennu's bulk density, Bennu's area-to-mass ratio, the masses of the 343 small-body perturbers, and a constant delay bias for the pseudo-range points. To these parameters, we add the parameters characterizing the fifth force, i.e., its range λ and strength $\widetilde{\alpha}$. We fix λ to 51 logarithmically spaced values between 10^{-2} au and 10^3 au, meaning that we have a total of 353 free parameters which are explicitly varied.

We perform a least-squares fit to Bennu optical and radar astrometry, and pseudo-range points discussed previously, explicitly varying all the parameters mentioned previously. For each of the fixed values of λ, we estimate all the model parameters, while focusing our discussion on $\widetilde{\alpha}$, which ultimately is the parameter we care about. As discussed below, we find that the inferred 95% confidence interval for $\widetilde{\alpha}$ is statistically compatible with $\widetilde{\alpha}=0$, and by extension, that analogous intervals for all the other parameters are in excellent agreement with their earlier estimates in ref. 4, whose force model assumed no fifth force. In other words, there is no evidence in the data for the presence of a fifth force affecting the motion of Bennu. A posteriori, this gives us further confidence in asserting that using pre-computed ephemerides and neglecting the fifth force interactions between couples of celestial bodies, which do not include Bennu, is indeed a good approximation. In the following (and in particular in Fig. 1), we adopt the common choice of only reporting 2σ upper limits on $\widetilde{\alpha}$.

Results and discussion

The outcome of the analysis detailed above is shown in Fig. 1, where we consider a fifth force model in which the mediator is either a dark photon A' of mass $m_{A'}$ or a baryon-coupled scalar field ϕ of mass m_ϕ, arising from a $U(1)_B$ local gauged symmetry. In this model, only the baryons feel the presence of the fifth force so that the couplings of the mediator to the proton and neutron are equal, $g_p = g_n$, while the coupling to the electron is zero, $g_e = 0$. We report 2σ upper limits on the dimensionless coupling $|\widetilde{\alpha}|$ versus the mediator mass $m_{\phi,A'}$ (lower horizontal axis), or equivalently the range of the fifth force λ (upper horizontal axis), using data from the OSIRIS-REx mission tracking the asteroid Bennu (green solid curve, with the green shaded region above the curve excluded). To provide a comparison, we ran the same analysis on the asteroid Apophis, using data available from optical and ground-based radar telescopes tracking its trajectory[43] (blue solid curve, once more with the blue shaded region above the curve excluded). Given the significantly enhanced sensitivity of the OSIRIS-REx mission at the meter-level scale, the constraints obtained when fitting this dataset (for Bennu's orbit) are currently much stronger than the constraints obtained with Apophis for $\lambda \gtrsim 3\times10^{-2}$ au, which is precisely the region we are featuring in Fig. 1.

The sensitivity we find is particularly strong in the region $10^{-18}\,\text{eV} \lesssim m_{\phi,A'} \lesssim 10^{-16}\,\text{eV}$, and is strongest for $m_{\phi,A'} \sim \mathcal{O}(10^{-17})\,\text{eV}$, which corresponds to a length scale $\lambda \sim \mathcal{O}(0.1)$ au. This is due to a combination of Bennu's eccentricity $\mathsf{e} \approx 0.20375$ and its semimajor axis $a = 1.1264$ au[4], which allows us to set some among the tightest constraints in the range $10^{-18}\,\text{eV} \lesssim m_{\phi,A'} \lesssim 10^{-17}\,\text{eV}$ when compared to planetary probes. In fact, the tracking of an asteroid orbiting with semimajor axis a and no eccentricity would translate into a fifth force constrain that peaks at the mass $m_{\phi,A'} \sim \hbar c/a$, which would correspond to $\sim 10^{-18}$ eV for an asteroid of semimajor axis same as Bennu's. The inclusion of the eccentricity makes the asteroid probe regions of the orbit that are smaller than a, with the closest approach to the Sun being $r_{\min} = a(1-\mathsf{e})/(1+\mathsf{e})$: this leads to the constraint shifting towards higher values of the mediator mass. The same reasoning applies to the results obtained with Apophis tracking data, whose eccentricity and semimajor axis are $\mathsf{e} \approx 0.1912$ and $a = 0.9224$ au respectively[44].

For length scales larger than $\hbar/(m_{\phi,A'}c)$, the Yukawa potential altering Eq. (6) can be expanded to yield a correction $\propto \lambda/\sqrt{\alpha}$. A fit to the results obtained gives:

$$10^{-13}\,\frac{\lambda/\text{km}}{\sqrt{\alpha}} \gtrsim 1.02\,, \tag{9}$$

where the result is valid at 2σ and for length scales $\lambda \gg$ au. Similar results have been obtained using INPOP ephemerides leading to $10^{-13}\,(\lambda/\text{km})/\sqrt{\alpha} > 1.83$[14] and $10^{-13}\,(\lambda/\text{km})/\sqrt{\alpha} > 3.93$[15] at 1σ and for a positive coupling strength α. For a comparison, the bound we obtained from using the Apophis ephemeris is $10^{-13}\,(\lambda/\text{km})/\sqrt{\alpha} > 4.79$ at 2σ.

Also shown in Fig. 1 are fifth force sensitivities obtained from other probes, including planetary motion (gray dash-dotted curve), which peaks for $m_{\phi,A'} \sim \mathcal{O}(10^{-18})$ eV, and was obtained by searching for an anomalous precession in the orbits of solar system planets[22]. The gray solid curve labeled "LLR" shows the sensitivity obtained from LLR probes of the anomalous precession of the Moon[21]. Other measurements based on the orbits of the Moon and the LAGEOS satellite, see e.g., ref. 45, place constraints on much shorter length scales, which are not shown in Fig. 1. The gray shaded area is excluded by the MICROSCOPE mission[46], which provides an accurate test of the weak equivalence principle (EP), improving over laboratory torsion balance experiments and atom interferometry measurements. Finally, the existence of a vector mediator in the mass range $6\times10^{-20}\,\text{eV} \lesssim m_{A'} \lesssim 2\times10^{-17}\,\text{eV}$ has been constrained by considerations on black hole superradiance[47] using spin measurements of supermassive black holes (SMBHs) from X-ray reflection spectroscopy[48]. We stress that these limits (enclosed between the two gray lines, as indicated by the two gray arrows, and only applying to the dark photon) should be interpreted with some caution for a number of reasons, including uncertainties inherent to the formation and spin evolution of SMBHs, the scarcity/reliability of other spin and mass measurements[49], as well as other considerations pertaining to the evolution of the superradiant instability in the presence of competing environmental effects[50,51].

The possibility that an ultra-light scalar of mass m_ϕ makes up a fraction or the totality of the dark matter has recently been tested in various ways, of which we here report a selected few. For instance, Cosmic Microwave Background anisotropy measurements set $m_\phi \gtrsim 10^{-24}\,\text{eV}$[52], which is tightened to $m_\phi \gtrsim 10^{-23}\,\text{eV}$ when including weak gravitational lensing measurements[53]. Very recently, the constraint $m_\phi \gtrsim 2.2\times10^{-21}\,\text{eV}$ has been reported analyzing stellar kinematical data for the Milky Way satellite galaxy Leo II[54]. At the opposite end of the mass spectrum, the bound $m_\phi \lesssim 10^{-19}\,\text{eV}$ has recently been obtained analyzing the motion of the S2 star around Sgr A*[55]. However, all these limits assume that the light boson contributes significantly to the dark matter budget (or potentially even makes up an entirety of the dark matter), an assumption which do not make explicitly, which is why we do not show these constraints in Fig. 1 (see also ref. 56 for some of the most stringent bounds on the axion-proton and axion-neutron couplings). The lack of such an assumption in our analysis makes our results somewhat more robust and model-independent – on the other hand, our results remain applicable to models of dark matter falling within the mass range in question. These points should be kept in mind when comparing our results to other limits in the literature.

For reference, we also compare our results to those obtained from the earlier qualitative sensitivity analysis for a sample of nine other asteroids in ref. 23, estimated solely from the precision in measuring the semimajor axes, eccentricities, and perihelia precessions of the asteroids whose properties were studied in ref. 57 (gray dashed curve). The bounds obtained in the present work are significantly more robust than those obtained in this earlier

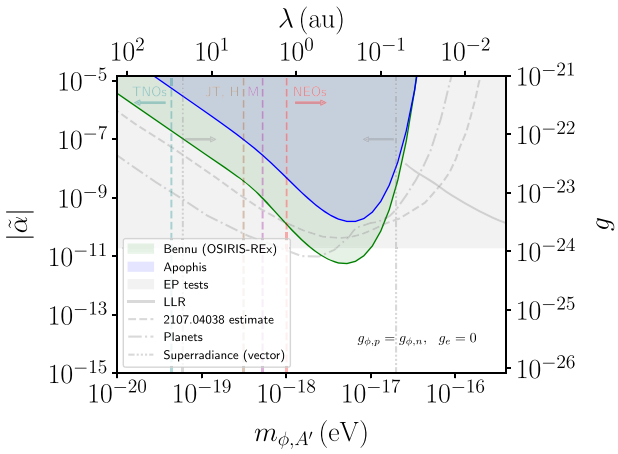

Fig. 1 | Constraints on the strength and range of fifth forces. The figure shows upper limits on the coupling strength of $U(1)_B$ dark photons A' and baryon-coupled scalars ϕ with $g_{\phi,p} = g_{\phi,n}$ and $g_e = 0$, as a function of the particle mass or, equivalently, its Compton wavelength. The limits have been obtained by analyzing the orbits of Bennu (green) and Apophis (blue), and the shaded regions above the respective curves are excluded. Also shown are upper limits from other probes: equivalence principle (EP) tests (gray shaded area is excluded)[46], lunar laser ranging (LLR, gray solid curve)[21], planetary precession (gray dash-dotted curve)[22], vector superradiance (excluding the region enclosed between the two gray lines)[47,62], and the earlier sensitivity reach estimated from the precessions of 9 asteroids (gray dashed curve)[23]. The four colored dashed vertical lines indicate the mass ranges indicatively probed by other classes of objects as per the colored labels: Jupiter Trojans (JT) and Hildas (H) in brown, main-belt asteroids (M) in magenta, Near-Earth Objects (NEOs) in red, and Trans-Neptunian Objects (TNOs) in teal.

qualitative analysis, given that the current analysis results from a direct fit to high-quality orbital tracking and constraints on the distance between Bennu and Earth, rather than condensing all of the information on the asteroid orbits into a single number, namely its orbital precession. Moreover, the software and force model used here (based on ref. 4) accounts for various non-gravitational effects, in addition to gravitational perturbations exerted by planets and the most massive asteroids, as a result significantly increasing the fidelity of the final constraints we have reported.

It is worth noting that after the first version of this work appeared online, ref. 37 derived upper limits on the coupling strengths of $U(1)_B$, $U(1)_{B\text{-}L}$ and $L_\mu - L_{e,\tau}$ gauge bosons using auxiliary channel data from LISA pathfinder, exploiting in particular the differential movement between test masses and spacecraft (see also ref. 58). The limits reported in ref. 37 are stronger than the ones we have obtained in the same mass region, and in any case competitive with ours—at the same time, however, these limits are derived under the additional assumption that the gauge boson makes up all the dark matter. For this reason, our results are an independent and complementary probe of the strength of fifth forces from the dynamics of objects in the solar system.

Finally, it is worth noting that modeling assumptions can potentially affect the estimates we have presented. When analyzing dark matter constraints from OSIRIS-REx data[24], the most significant effect in this sense was found to be caused by the choice of planetary ephemeris version, and we find that the same is true here. In particular, when switching from the DE424[59] to the DE440[60] ephemeris, we observe 0.1σ to 1.9σ shifts in the best-fit values of $\tilde{\alpha}$ (depending on the underlying value of λ). To capture this uncertainty floor, in Fig. 1, we have conservatively decided to report the formal 2σ upper limits, which therefore safely encompass the ephemeris-associated uncertainty budget.

Conclusions

We set constraints on hidden fifth forces and ultralight bosons using OSIRIS-REx tracking data for the asteroid Bennu. Based on its size and probability of future impacts with Earth, Bennu is one of the most potentially hazardous of all the currently known near-Earth asteroids, which is one of the reasons why meter-level tracking data is available. While we considered a model for the ultralight mediators for concreteness, our constraints can be translated into a wide class of models featuring Yukawa-type interaction. Our robust constraints on the fifth force strength are stronger than the existing laboratory and space tests bounds for the mediator mass range $m_{\phi,A'} \sim (10^{-18} - 10^{-17})$ eV. Although we have not explicitly assumed that the light bosons in question make up (all or part of) the dark matter, such models, including ones where the dark matter is extremely light or "fuzzy", are of course subject to the limits obtained through asteroid tracking.

The results presented here will be improved further in future work thanks to (i) the ephemeris that will be reported by the future OSIRIS-APEX mission in tracking Apophis; (ii) the inclusion of the data from tracking all other NEOs, TNOs, Trojans, Hildas, and main-belt asteroids. Including different classes of asteroids and solar-system objects enables the coverage of more orbital configurations, providing more comprehensive constraints on the fifth-force mediator masses that roughly correspond to the inverse of their semi-major axes. Further improvements on the data side may be achieved through the employment of quantum technologies, including technologies similar to the Deep Space Atomic Clocks, for example, which have also been considered to study dark matter and gravitational waves[61], among other science targets.

Data availability

All OSIRIS-REx data are archived in the Small Bodies Node of the Planetary Data System at https://sbn.psi.edu/pds/resource/orex/. Shape models of Bennu are available via the Small Body Mapping Tool (http://sbmt.jhuapl.edu/). Kernels and small-force files are available via NASA's Navigation and Ancillary Information Facility (https://naif.jpl.nasa.gov/pub/naif/ORX/).

Code availability

The analysis code is sensitive and proprietary to JPL property. A request to access the code can be made to Davide Farnocchia (Davide.Farnocchia@jpl.nasa.gov) and also requires approval from NASA JPL.

Received: 21 January 2024; Accepted: 14 August 2024;
Published online: 20 September 2024

References

1. Lauretta, D. S. et al. OSIRIS-REx: Sample return from asteroid (101955) bennu. *Space Sci. Rev.* **212**, 925–984 (2017).
2. Lauretta, D. S. et al. Spacecraft sample collection and subsurface excavation of asteroid (101955) Bennu. *Science* **377**, 285–291 (2022).
3. (JPL), N. J. P. L. *Small Bodies Node of the Planetary Data System.* https://sbn.psi.edu/pds/resource/orex/ (2022).
4. Farnocchia, D. et al. Ephemeris and hazard assessment for near-earth asteroid (101955) bennu based on OSIRIS-REx data. *Icarus* **369**, 114594 (2021).
5. Svrcek, P. & Witten, E. Axions in string theory. *JHEP* **06**, 051 (2006).
6. Arvanitaki, A., Dimopoulos, S., Dubovsky, S., Kaloper, N. & March-Russell, J. String axiverse. *Phys. Rev. D* **81**, 123530 (2010).
7. Visinelli, L. & Vagnozzi, S. Cosmological window onto the string axiverse and the supersymmetry breaking scale. *Phys. Rev. D* **99**, 063517 (2019).
8. Carone, C. D. & Murayama, H. Possible light U(1) gauge boson coupled to baryon number. *Phys. Rev. Lett.* **74**, 3122–3125 (1995).
9. Davidson, A. $B - L$ as the fourth color within an $SU(2)_L \times U(1)_R \times U(1)$ model. *Phys. Rev. D* **20**, 776 (1979).
10. Foot, R. New physics from electric charge quantization? *Mod. Phys. Lett. A* **6**, 527–530 (1991).
11. Izaguirre, E., Krnjaic, G. & Pospelov, M. Probing new physics with underground accelerators and radioactive sources. *Phys. Lett. B* **740**, 61–65 (2015).
12. Pospelov, M. & Tsai, Y.-D. Light scalars and dark photons in Borexino and LSND experiments. *Phys. Lett. B* **785**, 288–295 (2018).

13. Hassan, S. F. & Rosen, R. A. Resolving the ghost problem in non-linear massive gravity. *Phys. Rev. Lett.* **108**, 041101 (2012).
14. Bernus, L. et al. Constraining the mass of the graviton with the planetary ephemeris INPOP. *Phys. Rev. Lett.* **123**, 161103 (2019).
15. Bernus, L. et al. Constraint on the Yukawa suppression of the Newtonian potential from the planetary ephemeris INPOP19a. *Phys. Rev. D* **102**, 021501 (2020).
16. Burrage, C., Copeland, E. J. & Hinds, E. A. Probing dark energy with atom interferometry. *JCAP* **03**, 042 (2015).
17. Giannotti, M., Irastorza, I., Redondo, J. & Ringwald, A. Cool WISPs for stellar cooling excesses. *JCAP* **05**, 057 (2016).
18. Caldwell, A. et al. Dielectric haloscopes: a new way to detect axion dark matter. *Phys. Rev. Lett.* **118**, 091801 (2017).
19. Vagnozzi, S., Visinelli, L., Brax, P., Davis, A.-C. & Sakstein, J. Direct detection of dark energy: the XENON1T excess and future prospects. *Phys. Rev. D* **104**, 063023 (2021).
20. Vagnozzi, S. et al. Horizon-scale tests of gravity theories and fundamental physics from the event horizon telescope image of Sagittarius A. *Class. Quant. Grav.* **40**, 165007 (2023).
21. Hofmann, F. & Müller, J. Relativistic tests with lunar laser ranging. *Class. Quant. Grav.* **35**, 035015 (2018).
22. Kumar Poddar, T., Mohanty, S. & Jana, S. Constraints on long range force from perihelion precession of planets in a gauged $L_e - L_{\mu,\tau}$ scenario. *Eur. Phys. J. C* **81**, 286 (2021).
23. Tsai, Y.-D., Wu, Y., Vagnozzi, S. & Visinelli, L. Novel constraints on fifth forces and ultralight dark sector with asteroidal data. *JCAP* **04**, 031 (2023).
24. Tsai, Y.-D., Eby, J., Arakawa, J., Farnocchia, D. & Safronova, M. S. OSIRIS-REx constraints on local dark matter and cosmic neutrino profiles. *JCAP* **02**, 029 (2024).
25. Viswanathan, V., Fienga, A., Gastineau, M. & Laskar, J. *INPOP17a Planetary Ephemerides.* https://ui.adsabs.harvard.edu/abs/2017NSTIM.108.....V/abstract (2017).
26. Fienga, A. et al. *INPOP19a Planetary Ephemerides.* https://www.imcce.fr/content/medias/recherche/equipes/asd/inpop/inpop19a_20191214.pdf (2019).
27. Fienga, A. & Minazzoli, O. Testing theories of gravity with planetary ephemerides. *Living Rev. Rel.* **27**, 1 (2024).
28. Mariani, V., Fienga, A., Minazzoli, O., Gastineau, M. & Laskar, J. Bayesian test of the mass of the graviton with planetary ephemerides. *Phys. Rev. D* **108**, 024047 (2023).
29. DellaGiustina, D. et al. *OSIRIS-APEX: A Proposed OSIRIS-REx Extended Mission to Apophis*. https://www.hou.usra.edu/meetings/acm2023/pdf/2353.pdf (2022).
30. Clifton, T., Ferreira, P. G., Padilla, A. & Skordis, C. Modified gravity and cosmology. *Phys. Rept.* **513**, 1–189 (2012).
31. Giddings, S. B. & Strominger, A. Loss of incoherence and determination of coupling constants in quantum gravity. *Nucl. Phys. B* **307**, 854–866 (1988).
32. Coleman, S. R. Why there is nothing rather than something: a theory of the cosmological constant. *Nucl. Phys. B* **310**, 643–668 (1988).
33. Holdom, B. Two U(1)'s and epsilon charge shifts. *Phys. Lett. B* **166**, 196–198 (1986).
34. Wagoner, R. V. Scalar tensor theory and gravitational waves. *Phys. Rev. D* **1**, 3209–3216 (1970).
35. Adelberger, E. G., Heckel, B. R. & Nelson, A. E. Tests of the gravitational inverse square law. *Ann. Rev. Nucl. Part. Sci.* **53**, 77–121 (2003).
36. Schlamminger, S., Choi, K. Y., Wagner, T. A., Gundlach, J. H. & Adelberger, E. G. Test of the equivalence principle using a rotating torsion balance. *Phys. Rev. Lett.* **100**, 041101 (2008).
37. Frerick, J., Jaeckel, J., Kahlhoefer, F. & Schmidt-Hoberg, K. Riding the dark matter wave: novel limits on general dark photons from LISA pathfinder. *Phys. Lett. B* **848**, 138328 (2024).
38. HORIZONS System, JPL, NASA. *Trajectory in the Solar System From 9 August 2016 to 24 September 2023.* https://en.wikipedia.org/wiki/101955_Bennu#/media/File:Animation_of_OSIRIS-REx_trajectory.gif (2023).
39. Union, I. A. *Minor Planet Center*. https://minorplanetcenter.net/db_search/show_object?utf8=%E2%9C%93&object_id=101955 (2022).
40. N.J.P.L. *(JPL), Small-Body Radar Astrometry.* https://ssd.jpl.nasa.gov/?grp=num&fmt=html&radar= (2023).
41. Einstein, A., Infeld, L. & Hoffmann, B. The gravitational equations and the problem of motion. *Annals Math.* **39**, 65–100 (1938).
42. Will, C. M. *Theory and Experiment in Gravitational Physics* reversed edn, Vol. 400 (Cambridge University Press, 1993).
43. Farnocchia, D. & Chesley, S. R. Apophis trajectory, impact hazard, and sensitivity to spacecraft contact. In *Apophis T-7 Years: Knowledge Opportunities for the Science of Planetary Defense.* 2681 (LPI, 2022).
44. Brozović, M. et al. Goldstone and Arecibo radar observations of (99942) Apophis in 2012-2013. *Icarus* **300**, 115–128 (2018).
45. De Rujula, A. On weaker forces than gravity. *Phys. Lett. B* **180**, 213–220 (1986).
46. Touboul, P. et al. MICROSCOPE mission: final results of the test of the equivalence principle. *Phys. Rev. Lett.* **129**, 121102 (2022).
47. Baryakhtar, M., Lasenby, R. & Teo, M. Black hole superradiance signatures of ultralight vectors. *Phys. Rev. D* **96**, 035019 (2017).
48. Reynolds, C. S. Measuring black hole spin using x-ray reflection spectroscopy. *Space Sci. Rev.* **183**, 277–294 (2014).
49. Vagnozzi, S., Bambi, C. & Visinelli, L. Concerns regarding the use of black hole shadows as standard rulers. *Class. Quant. Grav.* **37**, 087001 (2020).
50. Brito, R., Cardoso, V. & Pani, P. Black holes as particle detectors: evolution of superradiant instabilities. *Class. Quant. Grav.* **32**, 134001 (2015).
51. Roy, R., Vagnozzi, S. & Visinelli, L. Superradiance evolution of black hole shadows revisited. *Phys. Rev. D* **105**, 083002 (2022).
52. Hlozek, R., Grin, D., Marsh, D. J. E. & Ferreira, P. G. A search for ultralight axions using precision cosmological data. *Phys. Rev. D* **91**, 103512 (2015).
53. Dentler, M. et al. Fuzzy dark matter and the dark energy survey year 1 data. *Mon. Not. Roy. Astron. Soc.* **515**, 5646–5664 (2022).
54. Zimmermann, T., Alvey, J., Marsh, D. J. E., Fairbairn, M. & Read, J. I. Dwarf galaxies imply dark matter is heavier than 2.2×10^{-21} eV *arXiv* https://doi.org/10.48550/arXiv.2405.20374 (2024).
55. Della Monica, R. & de Martino, I. Bounding the mass of ultralight bosonic dark matter particles with the motion of the S2 star around Sgr A*. *Phys. Rev. D* **108**, L101303 (2023).
56. Buschmann, M., Dessert, C., Foster, J. W., Long, A. J. & Safdi, B. R. Upper limit on the QCD Axion mass from isolated neutron star cooling. *Phys. Rev. Lett.* **128**, 091102 (2022).
57. Verma, A. K., Margot, J.-L. & Greenberg, A. H. Prospects of dynamical determination of general relativity parameter β and solar quadrupole moment $J_{2\odot}$ with asteroid radar astronomy. *Astrophys. J.* **845**, 166 (2017).
58. Miller, A. L. & Mendes, L. First search for ultralight dark matter with a space-based gravitational-wave antenna: LISA pathfinder. *Phys. Rev. D* **107**, 063015 (2023).
59. (JPL), N. J. P. L. *Solar System Dynamics*. https://ssd.jpl.nasa.gov//ftp/eph/planets/ioms/ (2023).
60. Park, R. S., Folkner, W. M., Williams, J. G. & Boggs, D. H. The JPL planetary and lunar ephemerides DE440 and DE441. *Astron. J.* **161**, 105 (2021).
61. Tsai, Y.-D., Eby, J. & Safronova, M. S. Direct detection of ultralight dark matter bound to the Sun with space quantum sensors. *Nature Astron.* **7**, 113–121 (2023).

62. Brito, R., Cardoso, V. & Pani, P. Superradiance: New frontiers in black hole physics. *Lect. Notes Phys.* **906**, 1–237 (2015).

Acknowledgements

We are grateful to Slava G. Turyshev, Cedric Delaunay, Olivier Minazzoli, Yotam Soreq, and Youjia Wu for useful discussions. Y.-D.T. is supported by the U.S. National Science Foundation (NSF) Theoretical Physics Program, grant No. PHY-1915005. Y.-D.T. thanks the CERN theory group for the short-term visitor program and generous support, and the Institute for Nuclear Theory at the University of Washington for its kind hospitality and stimulating research environment. This research was partly supported by the INT's U.S. Department of Energy grant No. DE-FG02-00ER41132. This work was partially performed at the Aspen Center for Physics, supported by National Science Foundation grant No. PHY-2210452. The National Science Foundation under Grant No. NSF PHY-1748958 partly supported this research. This research is partially supported by LANL's Laboratory Directed Research and Development (LDRD) program. YDT thanks the generous support from the LANL Director's Fellowship. D.F. conducted this research at the Jet Propulsion Laboratory, California Institute of Technology, under a contract with the National Aeronautics and Space Administration (80NM0018D0004). S.V. acknowledges support from the University of Trento and the Provincia Autonoma di Trento (PAT, Autonomous Province of Trento) through the UniTrento Internal Call for Research 2023 grant "Searching for Dark Energy off the beaten track" (DARKTRACK, grant agreement no. E63C22000500003), and from the Istituto Nazionale di Fisica Nucleare (INFN) through the Commissione Scientifica Nazionale 4 (CSN4) Iniziativa Specifica "Quantum Fields in Gravity, Cosmology and Black Holes" (FLAG). L.V. acknowledges support by the National Natural Science Foundation of China (NSFC) through the grant No. 12350610240 "Astrophysical Axion Laboratories", as well as the hospitality by the Galileo Galilei Institute for Theoretical Physics (Italy), the INFN Frascati National Laboratories (Italy), the INFN section of Trento (Italy), the INFN section of Ferrara (Italy), the INFN section of Napoli (Italy), and the Weinberg Institute for Theoretical Physics at the University of Texas in Austin, TX (USA) during the completion of this work. This publication is based upon work from COST Actions CA21106 – "COSMIC WISPers in the Dark Universe: Theory, astrophysics and experiments (COSMIC WISPers)" and CA21136 –"Addressing observational tensions in cosmology with systematics and fundamental physics (CosmoVerse)", both supported by COST (European Cooperation in Science and Technology).

Author contributions

D.F.: Conceptualization, investigation, formal analysis, data curation, writing-original draft, writing-review & editing, visualization, supervision. Y.-D.T., M.M., S.V., L.V.: Conceptualization, investigation, data curation, writing–original draft, writing–review & editing, visualization, supervision.

Competing interests

The authors declare no competing interests.

Additional information

Correspondence and requests for materials should be addressed to Yu-Dai Tsai or Luca Visinelli.

Peer review information *Communications Physics* thanks the anonymous reviewers for their contribution to the peer review of this work.